Intense convective systems in West Africa and their relationship to the African easterly jet

Karen I. Mohr* and Chris Thorncroft

Department of Earth and Atmospheric Sciences
University at Albany, SUNY

Submitted to *Quarterly Journal of the Royal Meteorological Society*, March 2005

*Corresponding author
Karen I. Mohr
Department of Earth and Atmospheric Sciences
University at Albany, SUNY
Albany, NY 12222-1000 USA
Tel: 1-518-442-4561
Fax: 1-518-442-5825
Email: mohr@atmos.albany.edu

Summary

Convective systems in West Africa were identified from observations by the Tropical Rainfall Measuring Mission satellite Microwave Imager at 85GHz for May-September 1998. Using reanalysis data, the 10-day average position of the African Easterly Jet (AEJ) for the same season was diagnosed from the 700hPa u-winds. For each convective system's centroid, the distance to the axis of the AEJ was calculated. The minimum brightness temperatures were ranked so that intense convective systems were defined as those in the 10^{th} percentile or lower. The weak (> 10^{th} percentile) and intense convective systems were represented statistically as two separate populations, the weak by the skewed Gumbel distribution and the intense by the symmetric normal distribution. From May to August, the peak in activity of weak convective systems remained south of 10°N but shifted east of 10°E. The peak in activity of the intense convective systems followed the seasonal migration of the AEJ northwards and became increasingly separate from the peak in activity of weak convective systems. The majority of both weak and intense convective systems occurred within 0.50deg of high terrain. The combination of orography and the high CAPE, high shear environment poleward of the AEJ appeared to be the most favorable environment for intense deep convection.

Keywords: West African monsoon, Sahel, Guinea Coast, JET2000 campaign, Saharan air layer

1. Introduction

The mid-tropospheric African easterly jet (AEJ) has been the focus of both idealized (e.g., Simmons 1977; Cook 1999; Thorncroft and Blackburn 1999) and observational studies (e.g., Burpee 1972; Reed *et al.* 1977; Parker *et al.* 2005). The classic view of the AEJ is that it arises in association with surface temperature gradients and thermal wind balance. Thorncroft and Blackburn (1999) described the two diabatically forced meridional circulations responsible for its maintenance, one north of the jet, associated with the surface fluxes and dry convection of the Saharan heat-low, the other south of the jet, associated with the deep moist convection in the intertropical convergence zone (ITCZ). Climatologically, the AEJ is poleward (about 15°N) of the summer rainfall maximum in West Africa, although many of the long-lived squall lines that traverse the region are observed to occur in the vicinity of the jet (e.g., Aspliden *et al.* 1976; Bolton 1984; Rowell and Milford 1993; Hodges and Thorncroft 1997). In this study, we analyse the frequency, location, and intensity of the convective systems occurring during May-September 1998 to learn where intense convective systems are most likely to occur with respect to the AEJ.

Observations made during the JET2000 experiment provide a new view of the dynamic and thermodynamic structure of the AEJ (Thorncroft et al. 2003). Using UK Meteorological Office research aircraft, dropsonde observations along and across the AEJ were made in the summer of 2000. Parker et al. (2005) used the JET2000 observations to deduce the thermodynamic structure of the AEJ environment. The conceptual model they developed is depicted in Fig. 1. The baroclinic zone around the AEJ is composed of three distinct layers, 1) a pseudo-adiabatic, moist monsoon layer at the lowest levels; 2) a dry-adiabatic, dusty, Saharan air layer (SAL) above it; 3) the rest of the troposphere above the SAL. Around the AEJ, there is

significant easterly vertical wind shear of the zonal wind in the low levels, switching to westerly wind shear in the mid-levels. In those areas where it occurs, the SAL functions as a capping inversion, permitting the accumulation of a large reservoir of convective available potential energy (CAPE) yet preventing the spontaneous release of conditional instability. Although the layering of moist then dry air may not be the only recipe for intense convection, in any region where these ingredients occur regularly, intense convection will be a feature of the regional climatology (Carlson and Ludlam 1968; Carlson *et al.* 1983; Emanuel 1994).

Parker et al. (2005) propose that the peak in activity of intense and of long-lived (> 6hr) convective systems will be in the most favorable combination of shear, CAPE, and convective inhibition poleward of the AEJ and poleward of the latitudes of peak rainfall, i.e., the ITCZ. Extrapolating from this hypothesis, convective systems in the ITCZ should be more frequent but tend to be weaker than the convective systems occurring poleward of the AEJ. To test the hypothesis of Parker and collaborators, we take advantage of microwave remote sensing data to distinguish intense from weak convection.

Data from the Tropical Rainfall Measuring Mission (TRMM) Microwave Imager (TMI) can be used for this purpose. Ice hydrometeors scatter 85GHz microwave radiation from the field of view of satellite-borne sensors. In 85GHz imagery, contiguous areas of depressed brightness temperatures indicate the presence of deep convection, and the value of the brightness temperatures are inversely correlated with the strength of the convective updraughts producing the ice hydrometeors (Spencer *et al.* 1989; Adler *et al.* 1991; McGaughey *et al.* 1996). Unlike IR imagery, 85GHz imagery can be used to make quantitative judgments about the intensity of deep convection. This allows it to be used to study the properties of convective systems at a

variety of spatial scales (e.g., Mohr and Zipser 1996; Mohr *et al.* 1999; Toracinta *et al.* 2002; Nesbitt and Zipser 2003).

We use TMI 85GHz data to study the convective systems of the wet season of 1998 and their relationship to the AEJ. The papers by Rowell and Milford (1993) and Hodges and Thorncroft (1997) on long-lived convective systems (squall lines) in West Africa discuss the important role of topography in their development. We consider the relationship of both weak and intense convective systems to topography and weigh the potential influence of the AEJ vs. topography. This research provides new insight into the relationship of the large-scale environment to the activity of intense convective systems.

2. Data and Methods

(a) The convective system database

The TMI ungridded data product from November 1997 to August 2001 has a resolution of 4.60km × 6.95km and a swath width of 759km. Mohr (2004) selected the wet seasons from 1998-2001 to create a database of convective systems from two years that were wetter than the long-term regional mean (1998 and 1999) and two years that were drier than the mean (2000 and 2001). The present study uses a sub-set, the wetter than average year 1998, of the convective system database from Mohr (2004). Because Mohr (2004) describes in detail the process of identifying convective systems and determining their properties, we merely summarize the methodology here:

- Horizontally and vertically polarized fields of 85 GHz brightness temperatures were converted into a polarization corrected temperature (PCT) to eliminate emissivity discontinuities due to surface type.

- A pattern recognition algorithm outlined areas of 4 or more contiguous pixels of PCT ≤ 255K in the region 3°N 17°W and 21°N 30°E.
- For each area, the Prabhakara et al. (2000) convective-stratiform discrimination algorithm was applied to determine convective system state of development (young, mature, or decaying) from the PCT gradients.
- Each system's date, time, location, size, minimum PCT, and other relevant properties were stored in a relational database.

Minimum PCT is a useful proxy for system intensity because several contiguous convective cells are required to generate enough large ice hydrometeors such as graupel and hail to depress the PCT below 225K in the TMI's field of view (McGaughey *et al.* 1996). Using all the convective systems in 1998, we calculated the 1^{st}, 2^{nd}, 5^{th}, 10^{th}, 25^{th}, and 50^{th} percentiles for minimum PCT. Table 1 contains the values of these percentiles, and each convective system was ranked according to Table 1. We define an *intense convective system* as having a minimum PCT in the 10^{th} percentile or lower. A *weak convective system* has a minimum PCT greater than the 10^{th} percentile.

The TRMM satellite makes six or more overpasses per day in the study region in Fig. 2. Because of this discrete sampling scheme, analysis in the present study is based on the accumulation of observations as TRMM precesses through the diurnal cycle and the statistical representation of the convective system population rather than tracking individual systems as in Hodges and Thorncroft (1997). In the strip-transect method of sampling used by forest biologists, the size of a population is estimated from counting species members in pre-defined strips of territory (US Forest Service 2004). Mohr et al. (1999) show that for a sufficiently large sample of convective systems, the confidence interval of this sampling technique will be small

enough to construct reliable cumulative distribution functions (CDF) of the intensities of regional convective system populations.

(b) Analyzing the African easterly jet

To diagnose the position and strength of the AEJ, we used 700 hPa u-wind data from the European Centre for Medium-Range Weather Forecasts (ECMWF) reanalysis (ERA40). The ERA40 product is T159 spectral resolution (1.125deg), 6hr temporal resolution, and has 23 constant pressure surfaces for 1957-2002. The ERA40 resolution of 1.125deg is approximately 125km in horizontal distance, not much larger in width than the smallest convective systems in the database.

Time-averaging of the zonal 700hPa winds was necessary to determine a representative position for the zonal jet. We chose a dekadal (10-day) average to eliminate the effect of synoptic influences associated with African easterly waves (e.g., Carlson 1969; Burpee 1972) and yet still represent meridional seasonal shifts in jet position. For 30-day months, the first dekad was days 1-10, the second days 11-20, and the third days 21-30. For 31-day months, the second dekad was days 11-21 and the third dekad days 22-31. The dekadal average 700hPa zonal wind field was the average at each point in the grid for all the days and times within the dekad. We defined the axis of the AEJ in each dekad by finding the latitude of the grid point with the minimum u-wind at each meridian from 18.0°W to 30.375°E. These meridians bounded the area for which convective systems were identified. In Tompkins (2005), the location, structure, and magnitude of the AEJ diagnosed from the ECMWF integrated forecast system was comparable to the AEJ diagnosed from JET2000 dropsonde data. Their results gave us confidence that our identification of the AEJ location would be sufficiently accurate to generate credible results in the present study.

The value of using a Geographic Information Systems (GIS) environment is the capability to overlay different sets of geographic data (themes) and analyse spatial relationships among features in different themes. In the GIS, the minimum distance from points in one theme to a line or polygon arc in another theme can be determined in map projection units. Our three themes were the 500m elevation contour (polygons), the AEJ axis (line), and the convective system centroids (points) occurring in the same dekad. For each dekad, the minimum distance in decimal degrees from each convective system centroid to the AEJ axis was added to the convective system database. If the centroid of the convective system was south of the jet, the distance was recorded as a negative number. Conversely, centroids north of the jet had positive distances. For all convective systems outside the 500m elevation contour, the distance to the nearest 500m contour was also added to the database. Convective systems whose centroids were located within the 500m contour were assigned 0.0deg, and convective systems farther than 2.0deg from high terrain were assigned a dummy value.

(c) Deriving the theoretical probability distributions

The GIS environment produced the variable "distance to the AEJ axis." Through grouping by ranks rather than the actual PCT values and then by month, we created large samples for statistical analysis. To fit a theoretical probability distribution, the sample size must be large enough to estimate accurately the distribution parameters such as the mean and standard deviation from the sample derived parameters.

We applied a sample size test to determine if each of our samples was large enough to estimate the population mean within a 95% confidence interval ($\alpha = 0.05$). Equation 1 gives the sample size n required to estimate the population mean at the desired precision (US Forest Service 2004).

$$n = 1.1164\left(\frac{3.8416s^2}{(\alpha\bar{x})^2}\right) + 7.8646 \quad (1)$$

The sample standard deviation and sample mean are s and $\bar{x}$, respectively. The coefficients were derived from the standard normal distribution. In those cases where the sample size was smaller than n, we combined samples so that, for example, instead of separate 1st and 2nd percentiles, there was a single 2nd percentile.

For sufficiently large samples, we fit several different continuous probability density functions (PDF) for -15.0deg ≤ x ≤ 15.0deg where x is the distance in decimal degrees from the AEJ. The results of a goodness of fit test determined the appropriate type of PDF. The goodness of fit test used was the Kolmogorov-Smirnov test because it can be applied to any theoretical distribution. This test compares the empirical and theoretical CDFs, and the null hypothesis is that the observed data fit the theoretical distribution. The maximum deviation between the CDFs is the Kolmogorov-Smirnov statistic which is then compared to a table of critical values to determine rejection. In the test's original form, the distribution parameters could not be estimated from the data sample. Crutcher (1975) devised a table of critical values that allows the use of sample-estimated parameters. In Crutcher's modified test, the critical value is $\nu N^{-½}$ where coefficient ν is specific to the distribution fitted, to α, and to the sample size N. The Kolmogorov-Smirnov statistic must be less than this critical value to retain the null hypothesis. In the next section, we discuss which distributions were appropriate for the data.

3. Results

(a) Convective systems and high terrain

Hodges and Thorncroft (1997) used IR data to track individual squall lines from genesis to lysis, identifying regions 1, 6, 8-10 on Fig. 2 as important genesis regions. Regions 2-5 and 7

are not listed as genesis regions. Because they are geographically and ecologically separate from the Dharfur Mountains (region 6), they will be referenced by their names.

In Fig. 3, convective systems ranked by minimum PCT from the 2nd dekads of (a) May and (b) August are plotted over a simplified elevation contour map. These months represent the beginning and the height of the wet season in the Sahel. In May, dense clusters of convective systems occur on the west sides of the Guinea Highlands, Jos Plateau, Cameroon Highlands, and Tondou Massif. Most of the more intense convective systems are south of 10°N, and few are far from the high terrain. Many of those far from high terrain occur in the coastal river valleys in the box 5°N 8°W-10°N 2°E. By August, there are convective systems clustering on the west sides of the Dharfur and Aïr Mountains and on the east side of the Jos Plateau. Compared to May, there are more intense convective systems occurring at greater distances from the high terrain in August. Most of August's intense convective systems are on the west side of the Dharfur Mountains and farther downwind in the vicinity of the 15th parallel. While May's intense convective systems are embedded within the area of peak convective system activity, most of August's intense convective systems are north of it. The separation between the peak activity of weak convective systems south of 10°N and the peak activity of intense convective systems north of 10°N is most apparent east of 10°E

Quantifying the relationship between high terrain and the location of convective systems involved using the GIS to find the distance to the nearest 500m elevation contour. The cumulative distribution functions (CDF) of distance from high terrain for the months of May and August are in Fig. 4. At least 50% of all convective systems in both months are located within 0.5deg of high terrain, and at least 75% are within 2deg. The weak systems in August and the intense systems in May have a stronger relationship with high terrain than their counterparts. In

Fig. 3b, there are so many weak convective systems plotted on top of each other on the Cameroon Highlands and the Tondou Massif that it is hard to see that in mid-August there are more weak convective systems in the region south of 10°N and east of 12°E than in the rest of the map combined. A smaller percentage of May's intense systems are located directly on top of high terrain, producing the small kink on the left-hand side of their curve in Fig. 4a.

August's intense convective systems and May's weak convective systems have the weaker relationship to high terrain. May's weak convective system CDF is influenced by the clusters of systems in the coastal river valleys and the scattered systems north of 15°N and west of 3°W. Moist surface conditions in the river valleys would make it possible for weak systems to develop in these areas. In the 925hPa wind fields (not shown here), the convective systems north of 15°N and west of 3°W occurred in areas of convergence associated with trailing mid-latitude troughs. In Fig. 5, the August intense convective system histogram varies less than 15% between bins 0.5-2.0deg, whereas May's decreases 25% or more from 0.5-2.0deg. Beyond 2.0deg are 23% of August's intense convective systems vs. 14% for May. Thus for August, Fig. 5 suggests that the probability that intense convective systems are 0.5deg or 2.0deg from high terrain is nearly the same, and that the probability that intense convective systems are far from high terrain is higher in August than in May.

For the sake of brevity, we do not include CDFs of the other months in the wet season. The CDFs of June, July, and September are intermediate to those of May and August. In July and September, the intense convective system CDF is underneath the weak convective system CDF, similar to August (Fig. 4b), but with a smaller gap.

(b) Convective systems and the AEJ

Figure 6 contains map views of the 700hPa u-wind fields for the 2nd dekads of each month of the wet season. The convective systems in Fig. 6 are ranked by their minimum PCT and plotted using the same legend as Fig. 3. In this series of maps, the seasonal changes in the position of the AEJ are apparent, as are preferred locations for convective systems to occur. Particularly in July through September, weak convective systems appear in great numbers south of the AEJ in the Cameroon Highlands-Tondou Massif region and around the Guinea Highlands. From May to August, the number of intense convective systems occurring north of the jet increases, and the intense convective system population appears to spread out zonally, downstream of the high terrain areas. Only in September are there more intense convective systems south of the jet. In both May and September, the clusters of intense convective systems are near the high terrain principally the Cameroon Highlands and southern Dharfur-northern Tondou.

To quantify the relationship between distance from the AEJ and intensity, we attempted to fit several different continuous distributions to each intensity rank. The PDFs for convective systems ranked by minimum PCT are in Fig. 7. Convective systems in the 1st percentile were grouped with those in the 2nd percentile so that "2%" is the PDF for all convective systems with a minimum PCT below 90K (Table 1). Based on the results of goodness of fit tests, two distributions consistently fit the same ranks each month, the normal (Gaussian) distribution for the intense convective systems (2-10%) and the Gumbel distribution for the weak convective systems (> 10%). The PDF for the normal distribution is given by

$$f(x) = \frac{1}{\sigma\sqrt{2\pi}} \exp\left\{ -\frac{(x-\mu)^2}{2\sigma^2} \right\} \qquad (2)$$

where the distribution parameters are the mean, μ, and standard deviation, σ, estimated from the sample mean and sample standard distribution.

Fitting with a normal distribution implies that the intense convective systems are symmetrically distributed about a mean position. From May through August, the peaks of the intense convective system curves are close to the ordinate, representing the axis of the AEJ. The 10% curve is just to the left of the 2% and 5% curves and tends to be broader, but it is still clearly distinguishable from the weak convective system curves. The separation between the cluster of intense convective system curves and the cluster of weak convective system curves first becomes apparent in June, as the area affected by seasonal rainfall expands. The separation peaks in August and then decreases when the ITCZ makes its seasonal retreat south. September is the only month where the peaks of all the intense convective system curves are to the left of the AEJ axis in Fig. 7e, but they are still separate from the weak convective system curves and close to the AEJ axis.

The Gumbel distribution, also known as the extreme value or Fisher-Tippett Type I distribution, is typically used for fitting datasets composed of extremes such as maximum or minimum temperatures. It is non-symmetric, with a fixed skewness of 1.14 and a fixed kurtosis of 5.4, appearing much like an exponential curve on one side and a normal curve with a heavy tail on the other side. The maximum case of the Gumbel distribution has the heavy tail on the right side. For the weak convective systems, only the Gumbel distribution produced Kolmogorov-Smirnov statistics below their critical values. The equation for the maximum case of the Gumbel distribution is

$$f(x) = \frac{1}{\beta}\exp\left[-\exp\left\{-\frac{(x-\xi)}{\beta}\right\} - \frac{(x-\xi)}{\beta}\right] \tag{3}$$

where β and ξ are the scale and location parameters, respectively (Wilks 1995; US Forest Service 2004). The scale and location parameters are estimated from the sample standard deviation, *s*, and sample mean, $\bar{x}$,

$$\hat{\beta} = \frac{s\sqrt{6}}{\pi} \tag{4}$$

$$\hat{\xi} = \bar{x} - \gamma\hat{\beta} \tag{5}$$

where γ is Euler's constant, 0.57721.

It was the lopsided shape of the Gumbel distribution rather than its customary use in extreme value analysis that prompted us to try to fit it to the weak convective system data. In Fig. 7, the peaks of the weak convective system curves appear progressively south of the AEJ axis as the number of weak convective systems in the southeast increases (Fig. 6). The scale parameter decreases 10% from May to August before increasing again in September. The heavy right-hand tail is heaviest for May followed by September. The configuration of the Gumbel distribution allows it to account for the scatter caused by intruding mid-latitude troughs in May and, later in the season, the occasional development of weak convective systems near the Adrar des Iforas, Aïr, and Tibesti Mountains, north of the concentration of weak convective systems associated with the ITCZ.

4. Discussion

Wilks (1995) gives three reasons for fitting a continuous PDF to a large dataset, reduction, smoothing/interpolation, and extrapolation. Given the large samples and wide geographic distribution of convective systems, all three reasons are applicable here. The PDFs make it possible to assert that weak convective systems, fit by a Gumbel distribution, are a different population from the intense convective systems, fit by a normal distribution. From their analysis of the AEJ environment in JET2000, Parker et al. (2005) propose that that the peak in activity of intense and of long-lived convective systems will be poleward of the AEJ and thus poleward of the latitudes of peak rainfall. At first glance, the position and separation of the

normal and Gumbel curves from June-August in Fig. 7 would appear to corroborate the hypothesis of Parker and collaborators.

That the intense convective system curves tend to be located at or just north of the AEJ axis between May and August confirm the expectation that the high CAPE, high shear AEJ environment is a favorable environment for intense deep convection. As the AEJ makes its northward progression from May to August, the peak in activity of the intense convective systems does also. It is also notable that from May to September, the area affected by intense convective systems expands. The standard deviations of the intense convective system curves increase 30%, suggesting that there is a non-negligible probability that they will be located equatorward of the AEJ axis. A potential source of scatter in the relationship between the AEJ axis and intense convective systems is the passage of synoptic-scale African easterly waves that may produce significant perturbations to the location of the mean AEJ position (Berry and Thorncroft 2005).

Weak convective systems represent a distinct population of convective systems with a different relationship to the AEJ and land surface state. In all months (May to September), the latitude of the peak activity of weak convective systems is always equatorward of the AEJ and does not move polewards with the AEJ. In May, weak convective systems occur in great numbers in humid coastal and river valley regions. Beginning in June, consistent with the strong influence of the Saharan heat-low, the ITCZ west of 10°E migrates north of 10°N in response to it. East of 10°E, away from the immediate influence of the Saharan heat-low, the peak activity of the weak convective systems and the ITCZ remain south of 10°N. When the western portion of the ITCZ migrates to low-lying areas with drier savanna grasslands and semi-desert land cover, the number of weak convective systems associated with the western ITCZ decreases. The

statistics of the weak convective systems in July and August are then dominated by the concentration of weak convective systems associated with the eastern ITCZ, located over high terrain and moister woody savanna and forest land cover. The results for the weak convective systems suggest that the local environment, influenced by surface conditions, is more important for the development of these systems than the AEJ.

Rowell and Milford (1993) and Hodges and Thorncroft (1997) identified certain areas of high terrain as important for the generation of long-lived convective systems. Since long-lived convective systems are but a small sub-set of the many convective systems that develop in these areas, it is not surprising to find that the majority of intense convective systems are less than 0.50deg of high terrain (Fig. 4), with the largest clusters occurring in the Dharfur Mountains (July-September), the Jos Plateau (May-September), and Cameroon Highlands (May and September). As the AEJ migrates polewards, different areas of orography become important. Thus, the Dharfur Mountains are significant only at the height of summer. Particularly in July and August, there appear to be many more intense convective systems that have propagated downstream away from orography, in this case, Dharfur. This is consistent with the view of the AEJ providing a favorable environment for the propagation of long-lived convective systems whether intense or not. The results in Fig. 4 are the product of the influence of the land surface state on weak convective systems and the AEJ on the intense convective systems, especially the sub-set of intense convective systems that are long-lived also.

Future study should explore the physical mechanisms of the interaction between the AEJ environment and topography in generating and then maintaining intense convective systems. This would seem to be a common scenario in the Dharfur Mountains north of 12°N, where the local climatology is a layered moist/dry humidity structure. The role of the humidity structure

further south in the Jos Plateau and Cameroon Highlands is less straightforward. The results for September (Fig. 7e) make this investigation particularly urgent, as it is the only month where the peaks of the intense convective system curves are slightly equatorward of the AEJ axis. Intense convective systems with some frequency (Fig. 6e) occur farther south of the AEJ in September than in any other month. An explanation of this phenomenon deserves its own paper.

5. Conclusion

Previous studies on West African convective systems have linked the generation of squall lines to certain areas of high terrain and the propagation of these systems to the favorable shears in the vicinity of the AEJ. In this study, we examined the particular relationship of intense convective systems to the AEJ, using TRMM Microwave Imager and ERA40 data for the wet season of 1998. Intense convective systems were defined as those in the 10^{th} percentile or lower for minimum PCT. For all convective systems, the distance to the axis of the AEJ from the ERA40 700hPa u-winds and the distance to the nearest 500m elevation contour were calculated to test the hypothesis that the peak in activity of intense convective systems is poleward of the AEJ axis.

The weak (> 10^{th} percentile) and intense convective systems were represented statistically as two separate populations, the weak fit by the skewed Gumbel distribution and the intense by the symmetric normal distribution. These fits were consistent for each rank from May to September. From May to August, there was an increasing separation in the peaks of activity of the weak and intense convective systems. The peak in activity of the intense convective systems shifted north from the Cameroon Highlands in May to the Dharfur Mountains by July, appearing poleward of the AEJ from May to August. By July the peak in activity of the weak convective systems occurred well south of the AEJ, in the area stretching from the Cameroon Highlands to

the Lake Victoria Highlands and the area around the Guinea Highlands. In September, the peak in activity of the intense convective systems was equatorward of the AEJ but closer to the AEJ than the peak in the weak convective systems.

Our results confirm the expectation that the high CAPE, high shear AEJ environment is a favorable environment for intense deep convection. The peak in activity of the intense convective systems followed the seasonal migration of the AEJ northwards. Convective systems south of the AEJ were more frequent but tended to be weaker. As the summer progressed, the peak in activity of weak convective systems remained south of 10°N, but had an important longitudinal variation, shifting east of 10°E. The longitudinal shift provides evidence that weak convective systems are more strongly influenced by the local environment determined by the interaction of the moist monsoon layer and the land surface state. The zonal spread of convective systems both intense and weak along the AEJ axis in mid-summer supports the view that the AEJ provides a favorable shear environment for the propagation of long-lived convective systems whether intense or not. How the AEJ environment interacts with topography and the land surface state to generate and then maintain intense and long-lived convective systems remains to be explored.

Acknowledgements. TRMM is co-sponsored by NASA and NASDA, the Japanese space agency, and the data are made available by the NASA-Goddard DAAC. The ECMWF ERA40 is available by agreement to the MSS at NCAR. We had valuable discussions with Chuck Alonge, Gareth Berry, Beth Mohr, Andy Negri, and Doug Parker. Thanks to Belinda Mex Moreno for drafting Fig. 1. The authors received financial support from NSF Grants 0215413 (Mohr) and 1023911 (Thorncroft).

References

Adler, R. F., Yeh, H.-Y. M., Prasad, N., Tao, W.-K., and Simpson, J., 1991: Microwave simulations of a tropical rainfall system with a three-dimensional cloud model. *J. Appl. Meteorol.*, **30,** 924-953

Aspliden, C. I., Tourre, Y., and Sabine, J. B., 1976: Some climatological aspects of West African disturbance lines during GATE. *Mon. Weather Rev.*, **104,** 1029-1035

Berry, G. J. and Thorncroft, C., 2005: Case study of an intense African easterly wave. *Mon. Weather Rev.***,** in press

Bolton, D., 1984: Generation and propagation of African squall lines. *Q. J. R. Meteorol. Soc.*, **110,** 695-721

Burpee, R. W., 1972: The origin and structure of easterly waves in the lower troposphere of North Africa. *J. Atmos. Sci.*, **29,** 77-90

Carlson, T. N. and Ludlam, F. H., 1968: Conditions for the occurrence of severe local storms. *Tellus*, **20,** 206-223

Carlson, T. N., 1969: Some remarks on African disturbances and their progress over the tropical Atlantic. *Mon. Weather Rev.*, **97,** 716-726

Carlson, T. N., Benjamin, S. G., Forbes, G. S., and Li, Y.-F., 1983: Elevated mixed layers in the regional severe storm environment: Conceptual model and case studies. *Mon. Weather Rev.*, **111,** 1453-1473

Cook, K. H., 1999: Generation of the African easterly jet and its role in determining West African precipitation. *J. Climate*, **12,** 1165-1184

Crutcher, H. L., 1975: A note on the possible misuse of the Kolmogorov-Smirnov test. *J. Appl. Meteorol.*, **14,** 1600-1603

Emanuel, K. A., 1994: *Atmospheric Convection*. Oxford University Press, 580 pp.

Hodges, K. I. and Thorncroft, C. D., 1997: Distribution and statistics of African mesoscale convective weather systems based on the ISCCP Meteosat imagery. *Mon. Weather Rev.*, **125,** 2821-2837

McGaughey, G. R., Zipser, E. J., Spencer, R. W., and Hood, R. E., 1996: High resolution passive microwave observations of convective systems over the tropical Pacific Ocean. *J. Appl. Meteorol.*, **35,** 1921-1947

Mohr, K. I. and Zipser, E. J., 1996: Mesoscale convective systems defined by their 85 GHz ice scattering signature: Size and intensity comparison over tropical oceans and continents. *Mon. Weather Rev.*, **124,** 2417-2437

Mohr, K. I., Famiglietti, J. S., and Zipser, E. J., 1999: The contribution to tropical rainfall with respect to convective system type, size, and intensity estimated from the 85-GHz ice scattering signature. *J. Appl. Meteorol.*, **38,** 596-606

Mohr, K. I., 2004: Interannual, monthly, and regional variability in the wet season diurnal cycle of precipitation in Sub-Saharan Africa. *J. Climate*, **17,** 2441-2453

Nesbitt, S. W. and Zipser, E. J., 2003: The diurnal cycle of rainfall and convective intensity according to three years of TRMM measurements. *J. Climate*, **16,** 1456-1475

Parker, D. J., Thorncroft, C. D., Burton, R., and Diongue, A., 2005: Analysis of the African easterly jet using aircraft observations from the JET2000 experiment. *Q. J. R. Meteorol. Soc.***,** in press

Prabhakara, C., R. Iacovazzi, J., Weinman, J. A., and Dalu, G., 2000: A TRMM microwave radiometer rain rate estimation method with convective and stratiform discrimination. *J. Meteorol. Soc. Jpn*, **78,** 241-258

Reed, R. J., Norquist, D. C., and Recker, E. E., 1977: The structure and properties of African wave disturbances as observed during Phase III of GATE. *Mon. Weather Rev.*, **105,** 334-342

Rowell, D. P. and Milford, J. R., 1993: On the generation of African squall lines. *J. Climate*, **6,** 1181-1193

Simmons, A. J., 1977: A note on the instability of the African easterly jet. *J. Atmos. Sci.*, **34,** 1670-1674

Spencer, R. W., Goodman, H. M., and Hood, R. E., 1989: Precipitation retrieval over land and ocean with the SSM/I: Identification and characteristics of the scattering signal. *J. Atmos. Oceanic Technol.*, **6,** 254-273

Thorncroft, C. D. and Blackburn, M., 1999: Maintenance of the African easterly jet. *Q. J. R. Meteorol. Soc.*, **125,** 763-786

Thorncroft, C. D., Parker, D. J., Burton, R. R., Diop, M., Ayers, J. H., Barjat, H., Devereau, S., Diongue, A., Dumelow, R., Kindred, D. R., Price, N. M., Saloum, M., Tayor, C. M., and Tompkins, A. M., 2003: The JET2000 Project: Aircraft observations of the African easterly jet and African easterly waves. *Bull. Am. Meteorol. Soc.*, **84,** 337-351

Tompkins, A. M., Diongue, A., Parker, D. J., and Thorncroft, C. D., 2005: The African easterly jet in the ECMWF integrated forecast system: 4DVar analysis. *Q. J. R. Meteorol. Soc.***,** in press

Toracinta, E. R., Cecil, D. J., Zipser, E. J., and Nesbitt, S. W., 2002: Radar, passive microwave, and lightning characteristics of precipitating systems in the Tropics. *Mon. Weather Rev.*, 802-824

US Forest Service, 2004: *Fuel and Fire Effects Monitoring Guide*. US Government Printing Office, 349 pp.

Wilks, D. S., 1995: *Statistical Methods in the Atmospheric Sciences: An Introduction.* International Geophysics Series no. 59, Academic Press, 467 pp.

Figures:

Figure 1: A conceptual model adapted from Parker *et al.* (2005) of the regional circulation during the wet season. The north-south vertical cross section along the Greenwich Meridian shows the seasonal mean locations of the AEJ and heat low. The Saharan air layer is in the wedge defined by isentropes A and B and the core of the AEJ. The convective clouds depict where shallow and deep cumulus clouds are likely to be found with respect to the regional circulation.

Figure 2: Topography in the study area, contoured at 200m, 500m, 700m, and 1000m. Regions of high (≥ 500m) terrain: (1) Guinea Highlands, (2) Adrar des Iforas, (3–5) Hoggar, Aïr, and Tibesti Mountains; (6) Dharfur Mountains, (7) Tondou Massif, (8) Lake Victoria Highlands, (9) Cameroon Highlands, (10) Jos Plateau.

Figure 3: Convective systems ranked by minimum PCT from the 2nd dekad of (a) May and (b) August are plotted on an elevation map simplified to show only the 500m contour. In the legend below the May map, the colors and sizes of the plotting points indicate the percentile rank of the minimum PCT. That is, the largest, darkest points are the most intense systems (top 1% rank), and the smallest, lightest points are the weakest systems (bottom 50% rank).

Figure 4: Cumulative distribution functions of distance (degrees) from high terrain for intense (filled squares) and weak (open triangles) convective systems in a) May and b) August. The CDFs were calculated using all convective systems occurring in each month. Distance from high terrain is defined as the distance from the system centroid to the nearest 500m elevation contour.

Figure 5: Histograms of May (hatched bars) and August (filled bars) intense convective systems 0.5deg or more from high terrain. Total number of intense convective systems: 240 in May and 251 in August.

Figure 6: 700hPa zonal winds and convective systems for the 2nd dekad May-September (a-e). Easterly winds are contoured with dashed lines and westerly with solid lines in 2ms^{-1} intervals. The -8 ms^{-1} contour is in bold. The blue line is the axis of the AEJ. Axis lines are not smooth due to the gridding of the reanalysis data.

Figure 7: The PDFs for each minimum PCT rank for May-September (a-e). The ordinate represents the axis of the AEJ, and the positions of convective systems are measured relative to it, north (positive) and south (negative). Solid lines are used for intense convective systems, dashed for weak.

Tables:

Table 1: Values for each percentile used in the analysis.

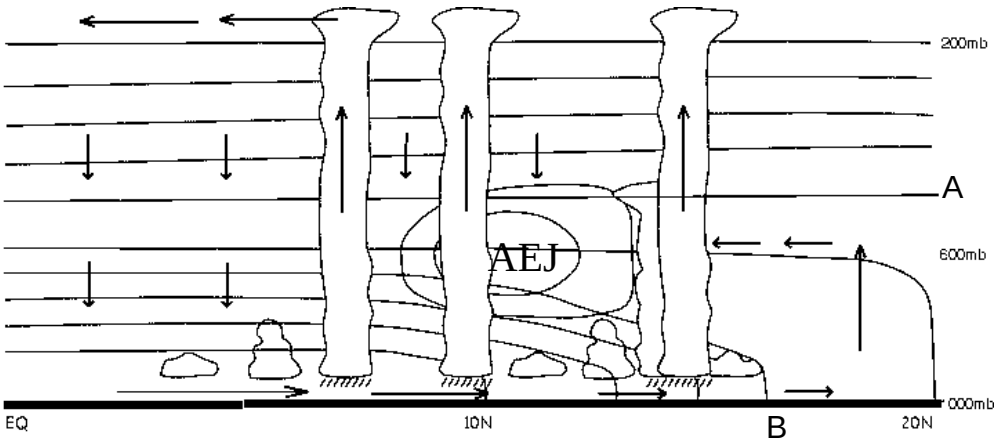

Figure 1: A conceptual model adapted from Parker *et al.* (2005) of the regional circulation during the wet season. The north-south vertical cross section along the Greenwich Meridian shows the seasonal mean locations of the AEJ and heat low. The Saharan air layer is in the wedge defined by isentropes A and B and the core of the AEJ. The convective clouds depict where shallow and deep cumulus clouds are likely to be found with respect to the regional circulation.

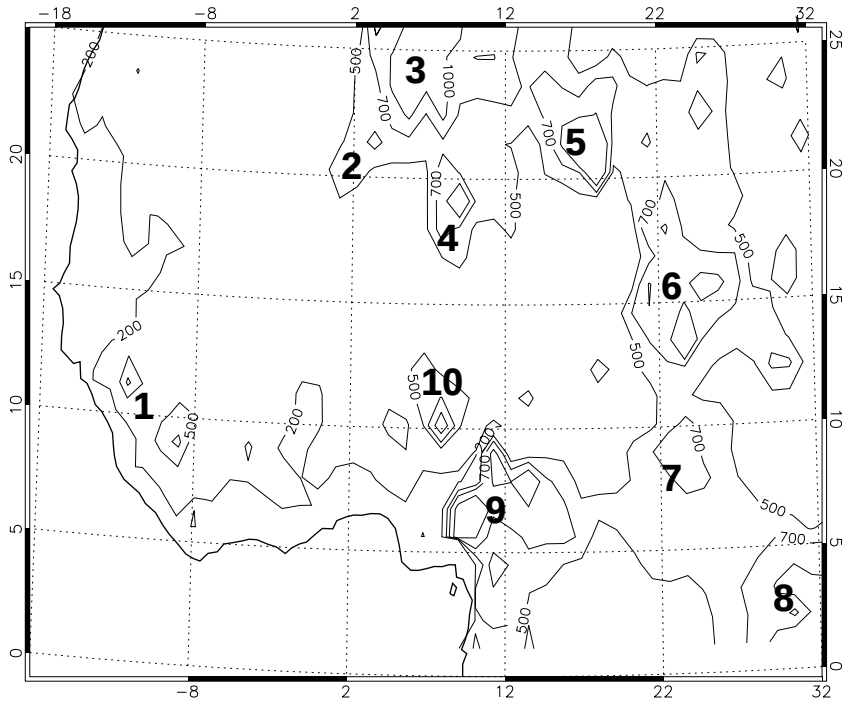

Figure 2: Topography in the study area, contoured at 200m, 500m, 700m, and 1000m. Regions of high (≥ 500m) terrain: (1) Guinea Highlands, (2) Adrar des Iforas, (3–5) Hoggar, Aïr, and Tibesti Mountains; (6) Dharfur Mountains, (7) Tondou Massif, (8) Lake Victoria Highlands, (9) Cameroon Highlands, (10) Jos Plateau.

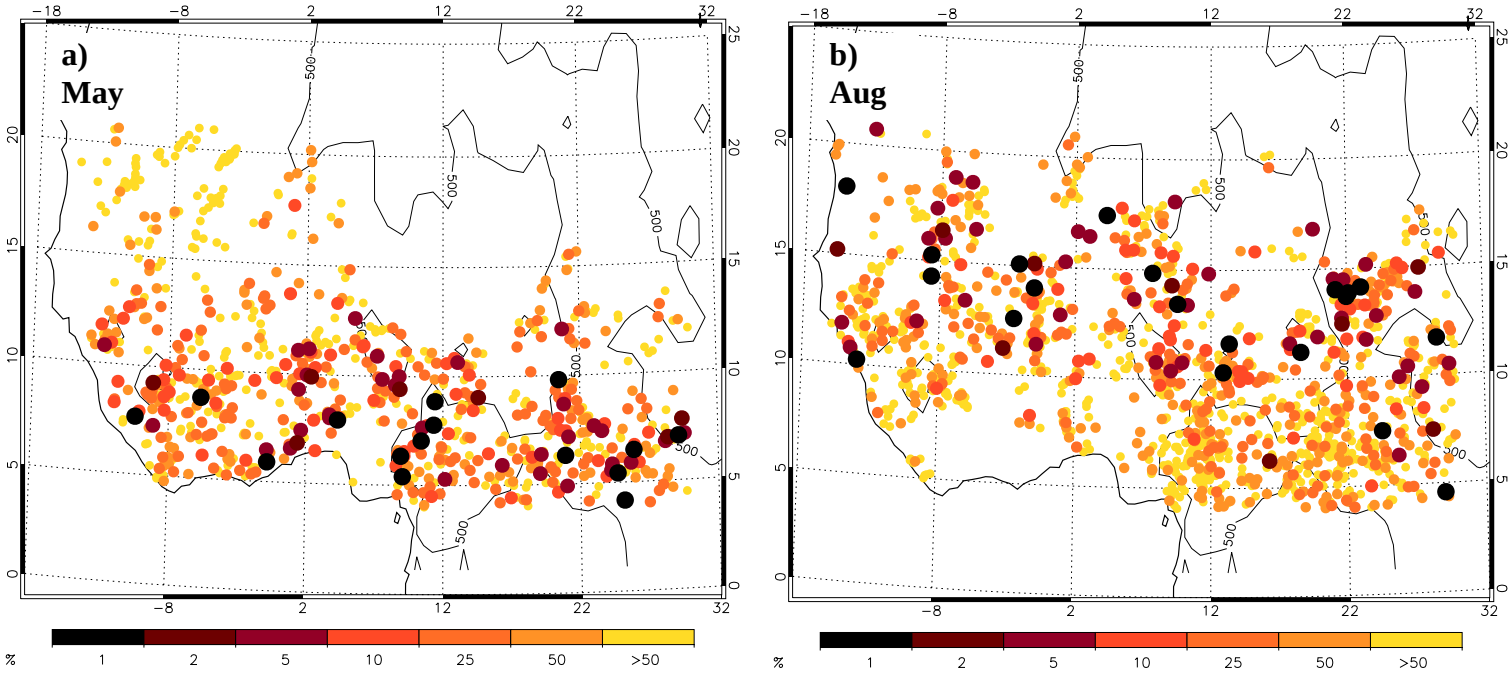

Figure 3: Convective systems ranked by minimum PCT from the 2nd dekad of (a) May and (b) August are plotted on an elevation map simplified to show only the 500m contour. In the legend below the May map, the colors and sizes of the plotting points indicate the percentile rank of the minimum PCT. That is, the largest, darkest points are the most intense systems (top 1% rank), and the smallest, lightest points are the weakest systems (bottom 50% rank).

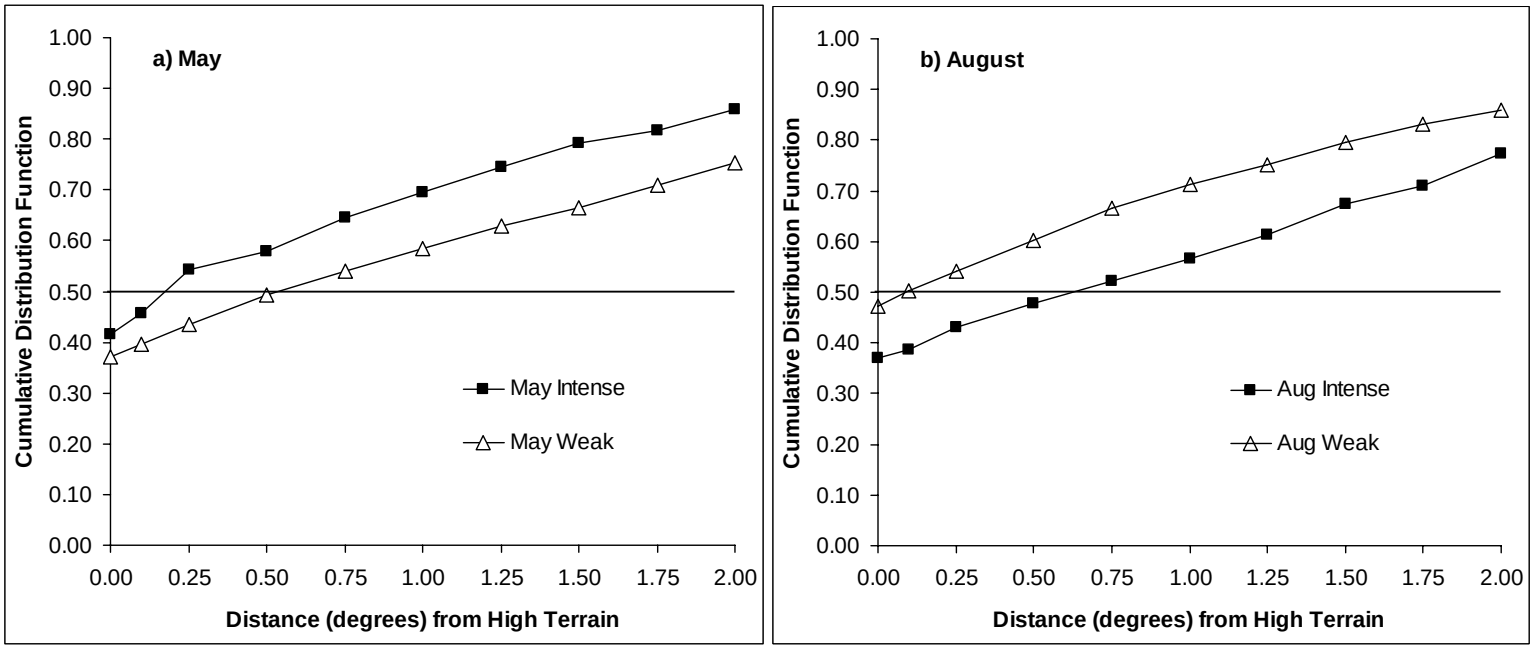

Figure 4: Cumulative distribution functions of distance (degrees) from high terrain for intense (filled squares) and weak (open triangles) convective systems in a) May and b) August. The CDFs were calculated using all convective systems occurring in each month. Distance from high terrain is defined as the distance from the system centroid to the nearest 500m elevation contour.

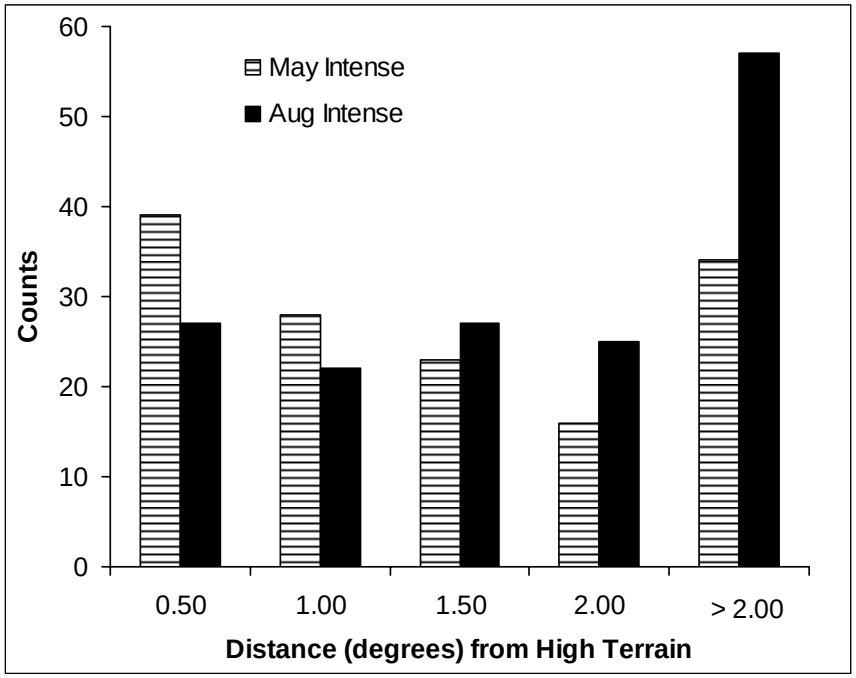

Figure 5: Histograms of May (hatched bars) and August (filled bars) intense convective systems 0.5deg or more from high terrain. Total number of intense convective systems: 240 in May and 251 in August.

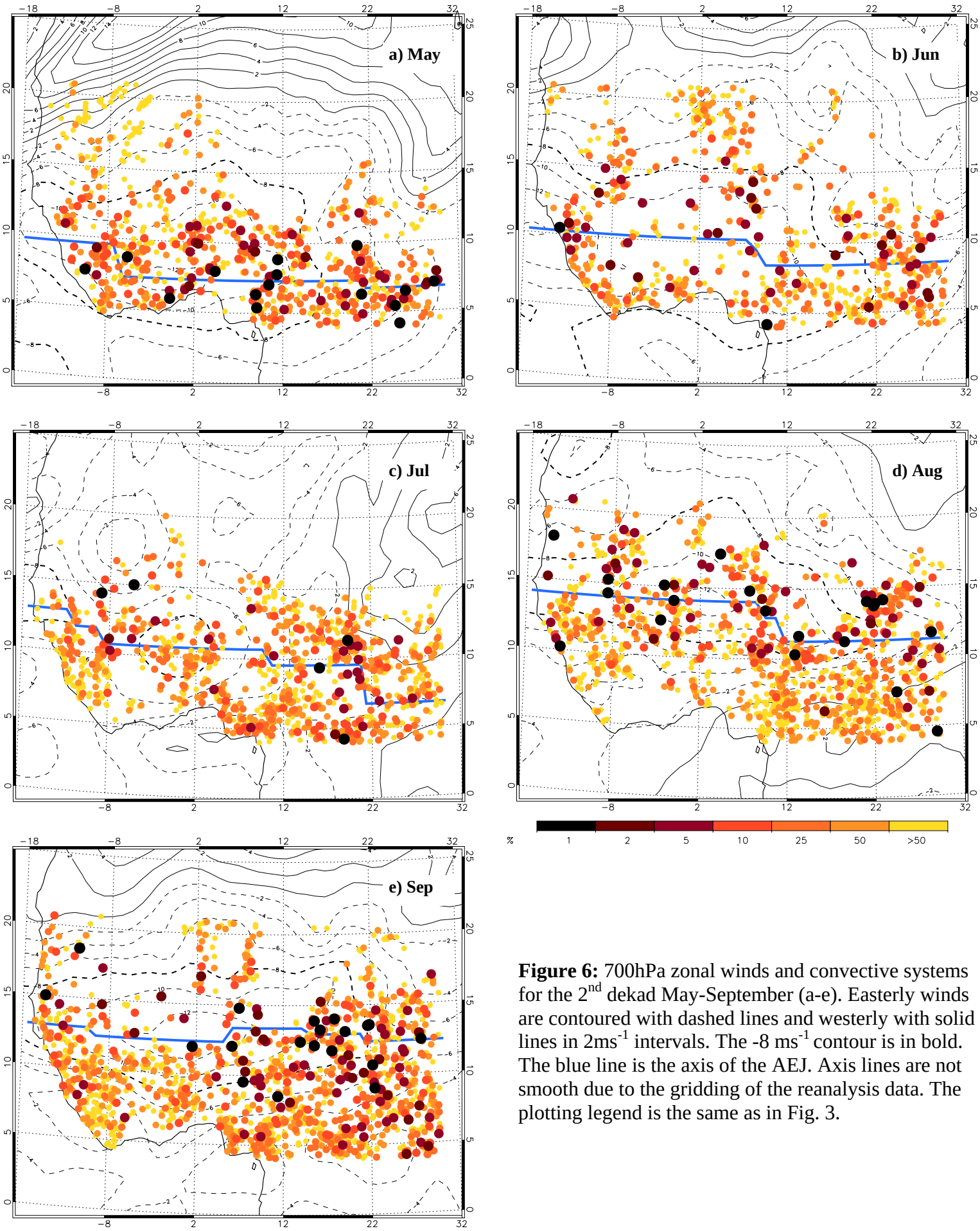

Figure 6: 700hPa zonal winds and convective systems for the 2nd dekad May-September (a-e). Easterly winds are contoured with dashed lines and westerly with solid lines in 2ms^{-1} intervals. The -8 ms^{-1} contour is in bold. The blue line is the axis of the AEJ. Axis lines are not smooth due to the gridding of the reanalysis data. The plotting legend is the same as in Fig. 3.

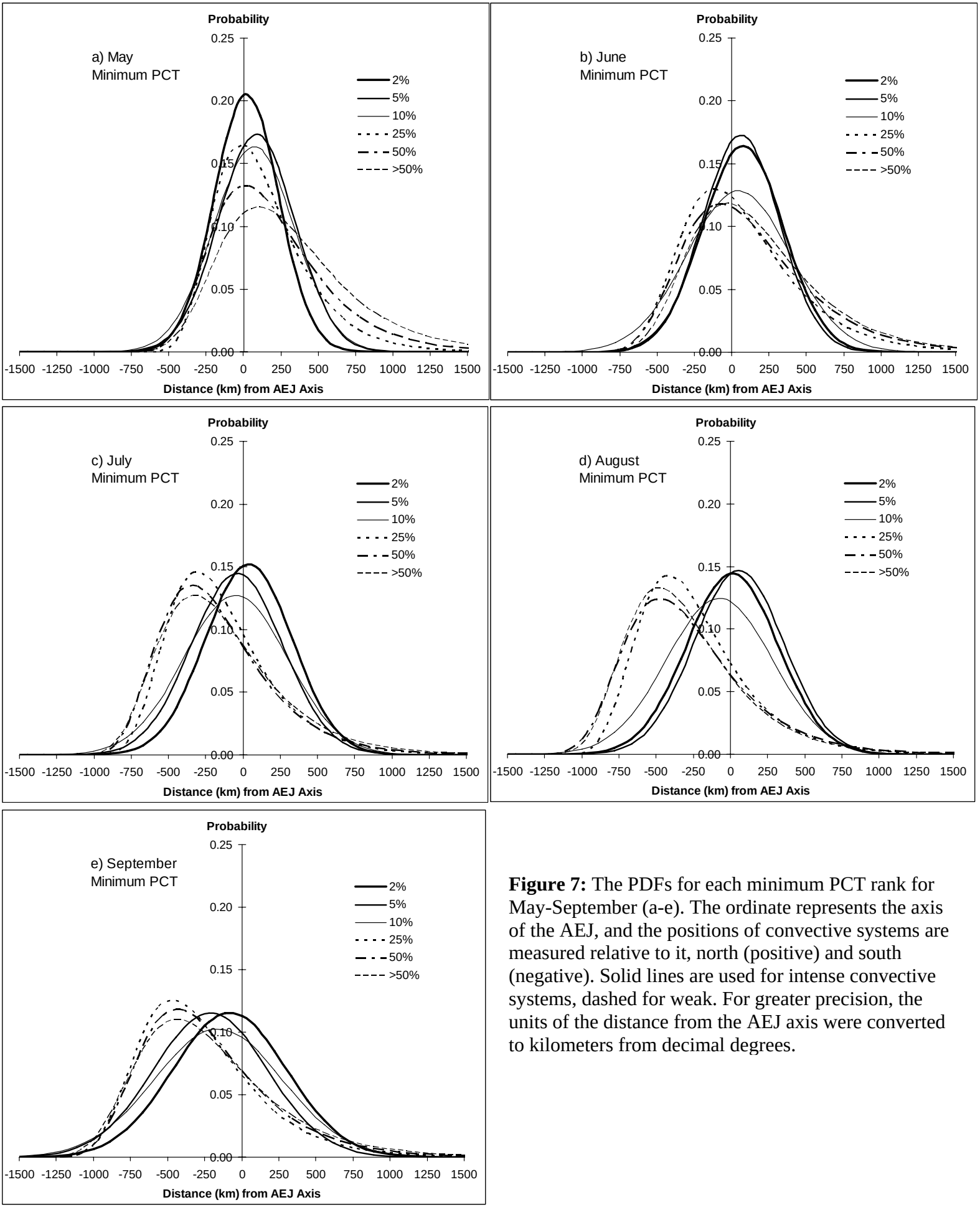

Figure 7: The PDFs for each minimum PCT rank for May-September (a-e). The ordinate represents the axis of the AEJ, and the positions of convective systems are measured relative to it, north (positive) and south (negative). Solid lines are used for intense convective systems, dashed for weak. For greater precision, the units of the distance from the AEJ axis were converted to kilometers from decimal degrees.

Table 1: Values for each percentile used in the analysis.

Percentile Rank	Min PCT (K)
1st	80
2nd	90
5th	110
10th	135
25th	180
50th	225